Synthesis and Characterization of Poly(trimethylene terephthalate) Nanocomposites Incorporating Multi-Walled Carbon Nanotubes

Chin-San Wu

Department of Chemical and Biochemical Engineering, Kao Yuan University, Kaohsiung County 82101, Taiwan, Republic of China

Received 26 February 2009; accepted 13 May 2009
DOI 10.1002/app.30754
Published online 23 June 2009 in Wiley InterScience (www.interscience.wiley.com).

ABSTRACT: Poly(trimethylene terephthalate) (PTT) nanocomposites containing multi-walled carbon nanotubes (MWNTs) were prepared using a melt-blending process. Acrylic acid-grafted PTT (PTT-*g*-AA) and multihydroxyl-functionalized MWNTs (MWNTs−OH) were used to improve the compatibility and dispersibility of MWNTs within the PTT matrix. The nanocomposites were characterized morphologically by transmission electron microscopy and chemically using Fourier transform infrared absorbance, ^{13}C solid-state nuclear magnetic resonance, and ultraviolet-visible spectroscopy. The thermal and mechanical properties of the blends were also evaluated. The functionalized PTT-*g*-AA/MWNT–OH blend showed markedly enhanced thermal and mechanical properties due to the formation of ester bonds from the condensation of the carboxylic acid groups of PTT-*g*-AA with the hydroxyl groups of MWNT–OH. The optimal proportion of MWNT–OH in the blends was 1 wt %. In excess of this amount, compatibility between the organic and inorganic phases was compromised. © 2009 Wiley Periodicals, Inc. J Appl Polym Sci 114: 1633–1642, 2009

Key words: carbon nanotubes; blends; PTT; nanocomposites

INTRODUCTION

The substitution of biological materials for fossil fuel-based materials has become an urgent goal. Fully renewable resource-based materials have the advantage of eco-friendliness but may not satisfy all the performance requirements in industrial applications. Polymers and other materials derived from mixed renewable and fossil fuel sources are effective in alleviating fossil fuel dependency and can deliver the desired performance using a more sustainable stock material. Poly(trimethylene terephthalate) (PTT) is a three-carbon glycol terephthalate (3GT) and a condensation polymer (Scheme 1). It is manufactured from 1,3-propanediol, available from renewable corn sugar, and dimethyl terephthalate (DMT) derived from fossil fuel.

PTT, along with poly(ethylene terephthalate) (PET) and poly(butylene terephthalate) (PBT), belongs to the thermoplastic aromatic polyester family. Although PTT has been studied for decades, particularly within the textile industry, it has not been commercialized due to its high cost.[1–4] Studies have suggested that manufacturing 1,3-propanediol from renewable resources, such as corn, could expedite the commercialization process. Given its high elasticity and recovery characteristics, PTT fibers are applicable in garments requiring good resilience and can be used as a substitute for nylon in carpets and other coverings.[5–8] In addition, PTT has been used as an engineering thermoplastic due to its excellent thermal and mechanical properties. Multicomponent polymer systems, incorporating PTT with materials such as poly(ethylene naphthalate), poly(ether imide), polystyrene, and polycarbonate, have been reported.[9–11] Although many studies have focused on the crystal structure and chemical structure of PTT, few have explored the mechanical properties and processing of PTT composites reinforced with inorganic fillers.[12,13] Recent research has suggested that inorganic fillers can significantly improve the mechanical properties of PTT. Modifying the surface of the inorganic filler could potentially enhance adhesion with the polymer matrix.

In the past decades, inorganic clays such as montmorillonite and hectrite have been used as reinforcement materials in polymers due to their nanoscale size and intercalation/exfoliation properties.[14–16] At the nanoscale, inorganic fillers can dramatically improve the macroscopic physical and mechanical properties of the polymer blend, though the total amount of filler material is small. Since the discovery

Correspondence to: C.-S. Wu (cws1222@cc.kyu.edu.tw).

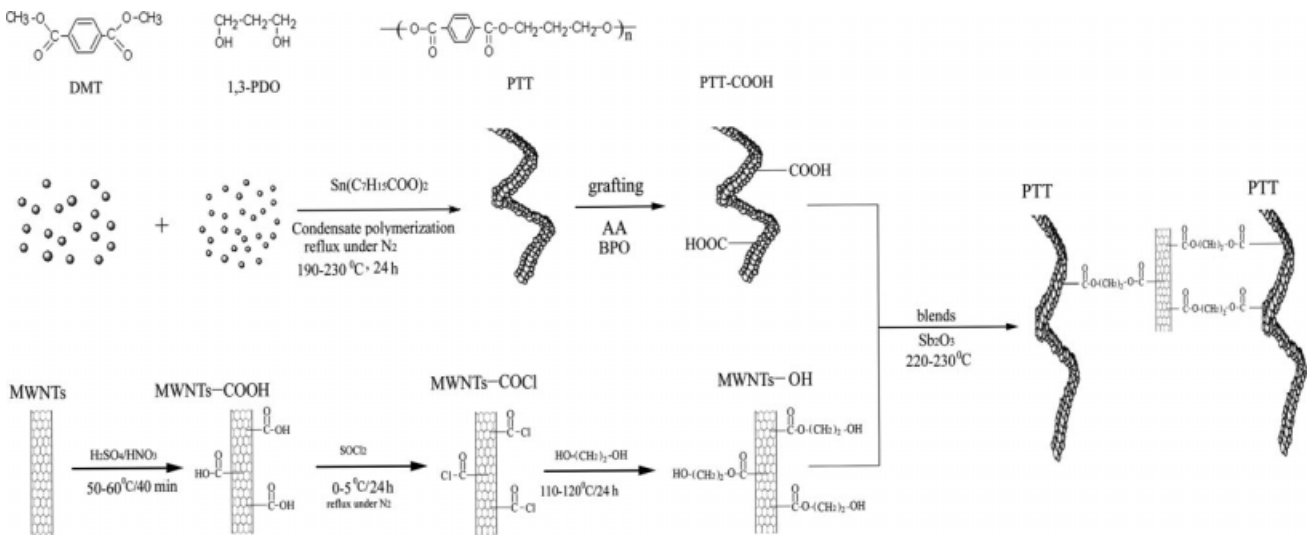

Scheme 1 The synthesis and modification of PTT and MWNTs, and the procedure used to prepare the blends.

of carbon nanotubes (CNTs) by Iijima,[17] extensive research has been devoted to the application of CNTs as inorganic fillers.[18–21] However, obtaining a uniform dispersion of CNTs in the polymer matrix is challenging due to the insolubility of CNTs and the inherently poor compatibility between the two phases. Inhomogeneous nanocomposites often do not meet performance specifications. Consequently, several methods have been proposed in which the phase compatibility between the CNTs and the polymer matrix was enhanced by functionalization of the nanotubes themselves, e.g., by anchoring to the matrix polymer. The oxidative generation of carboxylic acid groups at the surface of CNTs, followed by covalent linkage of these groups to matrix oligomers or polymers, has been shown to be effective.[22–28] Generally, covalent linkage to CNTs is more stable and effective than noncovalent bonds. Therefore, carboxylic acid groups formed at the ends and in defect sites of CNTs are most commonly used for precursor functionalization to facilitate the formation of ester bonds and organometallic structures.[29,30]

The current study investigated the effects of functionalized inorganic filler on the chemical and mechanical properties of PTT-based nanocomposite materials. To our knowledge, multi-walled CNTs (MWNTs) have not been systematically evaluated as a reinforcement material in PTT to produce biodegradable nanocomposites. This report describes the preparation and characterization of PTT/MWNT nanocomposite materials.

EXPERIMENTAL METHODS

Materials

MWNTs (purity >95%, diameter = 20–40 nm) produced via chemical vapor deposition (CVD) were purchased from Seasunnano Pro. Co. (Nanjing, China). Sulfuric acid (96%), nitric acid (61%), thionyl chloride, ethylene glycol, 1,3-propanediol, dimethyl terephthalate (DMT), and acrylic acid (AA) were obtained from Aldrich Chemical Co. (Milwaukee, WI). The AA was purified before use by recrystallization from chloroform. The initiator used in this study was benzoyl peroxide (BPO; Aldrich Chemical Co.), which was purified by dissolution in chloroform and reprecipitation in methanol. Other reagents were purified using conventional methods.

Synthesis of PTT

The DMT, 1,3-propanediol (PDO) and $Sn(C_7H_{15}COO)_2$ were mixed and autocalved by a weight ratio of 2 : 1 : 0.0005, respectively. Excess PDO (10 wt %) was added to drive the reaction to completion and $Sn(C_7H_{15}COO)_2$ was added as a catalyst. The reaction mixture was heated to 190–200°C for 12 h and stirred under a mild stream of nitrogen to generate an ester-interchange reaction. In theory, over 95% of the methanol should be released during the reaction process, resulting in the formation of bis-hydroxypropyl terephthalate. The mixture was then heated to 220–230°C for 2 h and the pressure was gradually reduced to less than 1 Torr to remove excess PDO. The polycondensation reaction was allowed to proceed for 10 h with continual removal of the PDO by-product. Molecular weigth (Mw) of PTT is 3.36×10^4 estimated by gel permeation chromatography.

Grafting reaction and sample preparation

A mixture of AA and BPO was added in four equal portions at 2 min intervals to molten PTT to allow

grafting to take place. The reactions were carried out under a nitrogen atmosphere at 45 ± 2°C. Preliminary experiments showed that reaction equilibrium was attained in less than 10 h, and reactions were therefore allowed to progress for 10 h, at a rotor speed of 60 rpm. The product (4 g) was dissolved in 200 mL of refluxing $CF_3COOD/CDCl_3$ (80/20, v/v) at 45 ± 2°C, and the solution was then filtered through several layers of cheesecloth. The $CF_3COOD/CDCl_3$-soluble product in the filtrate was extracted five times, using 600 mL of cold acetone for each extraction.

Determination of grafting percentage

By means of a titration method, the acrylic acid loading of the $CF_3COOD/CDCl_3$-soluble polymer was calculated from the acid number, and the result was expressed as the grafting percentage. About 2 grams of copolymer was heated for 2 h in 200 mL of refluxing $CF_3COOD/CDCl_3$. This solution was then titrated immediately with a 0.03 *N* ethanolic KOH solution, which had been standardized against a solution of potassium hydrogen phthalate, with phenolphthalein used as an indicator. The acid number and the grafting percentage could then be calculated using the following equations:[31]

$$\text{Acid number(mg KOH/g)} = \frac{V_{KOH}(\text{mL}) \times C_{KOH}(\text{N}) \times 56.1}{\text{polymer(g)}} \quad (1)$$

$$\text{Grafting percentage (\%)} = \frac{\text{Acid number} \times 72}{2 \times 561} \times 100\% \quad (2)$$

With BPO loading and AA loading kept at 0.3 wt % and 10 wt %, respectively, the percentage grafting was determined as 5.52 wt %.

Preparation of MWNT–OH

The modification of MWNT and PTT and the preparation of nanocomposite blends are illustrated in Scheme 1. Approximately 500 mg of crude MWNTs was stirred in 30 mL of a concentrated H_2SO_4/HNO_3 (1 : 3) mixture at 50–60°C for 40 min to oxidatively generate carboxyl functional groups. During this process, the MWNT volume expanded several-fold, suggesting that many of the MWNT bundles were exfoliated into individual nanotubes.[32] MWNTs with pendant carbonyl chloride groups (MWNT–COCl) were obtained by refluxing thionyl chloride with the acid-treated samples (MWNT–COOH) at 0–5°C for 24 h. The conversion of carboxylic acids into acid chlorides was accompanied by the formation of gaseous SO_2 and HCl. SO_2 was continuously removed to lower the extent of the reverse reaction. After the reaction was complete, unreacted $SOCl_2$ was evaporated with a rotary evaporator, and the MWNT–COCl samples were dried in a vacuum oven overnight. MWNT–COCl samples were highly reactive and kept isolated from ambient air to prevent unintentional hydrolysis of the −COCl groups into carboxylate ions. MWNT–COCl was reacted with ethylene glycol at 110–120°C for 24 h to yield hydroxyl-functionalized MWNTs (MWNT–OH). MWNT–OH was separated by vacuum filtration through a 0.22-μm polycarbonate membrane filter (Millipore, Billerica, MA) and subsequently washed with anhydrous xylene. After repeated washing and filtration steps, the solid MWNT−OH was dried overnight in a vacuum oven.

Preparation of hybrids

Blends were prepared using a "Plastograph" 200 Nm W50EHT mixer with a blade-type rotor (C.W. Brabender Instruments, Hackensack, NJ). Prior to blending, MWNT and MWNT−OH samples were dried in a vacuum oven at 60°C for 2 days. Blends of PTT/MWNT or PTT-*g*-AA/MWNT−OH hybrid blends were prepared with 0, 0.5, 1.0, 1.5, and 2.0 wt % inorganic filler. About 20 g of mixture (polymer and filler) was mixed at 50 rpm and 220–230°C for 30 min with a Sb_2O_3 catalyst. For PTT-*g*-AA/MWNT−OH, the blended mixture was then placed in a vacuum oven at 105°C for 8 h to continue the esterification reaction between PTT-*g*-AA and MWNT–OH. Standard specimens were prepared by pressing the hybrid blends into plates 1 mm thick using a hydrolytic press at 220°C and 100 atm. After pressing, the plates were placed in a dryer for cooling. Prior to characterization, the specimens were conditioned at a relative humidity of 50 ± 5% for 24 h.

Characterizations of hybrid blends

Fourier transform infrared spectrometry (FTIR; FTS-7PC type; Bio-Rad, Hercules, CA) was used to investigate the grafting reaction of AA onto PTT and to verify ester bond formation between the MWNT−OH phase and the PTT matrix. Samples subjected to FTIR analysis were ground into fine powders in a milling machine and pressed into pellets with KBr. Solid-state ^{13}C nuclear magnetic resonance (NMR) analyses were performed with an AMX 400 ^{13}C NMR spectrometer (Bruker, Madison, WI) at 100 MHz. ^{13}C NMR spectra were acquired under cross-polarization and magic angle sample spinning. Power decoupling was employed with a 90° pulse and 4 s cycle time. Ultraviolet-visible (UV-vis) absorption spectra were recorded on a UV2001-

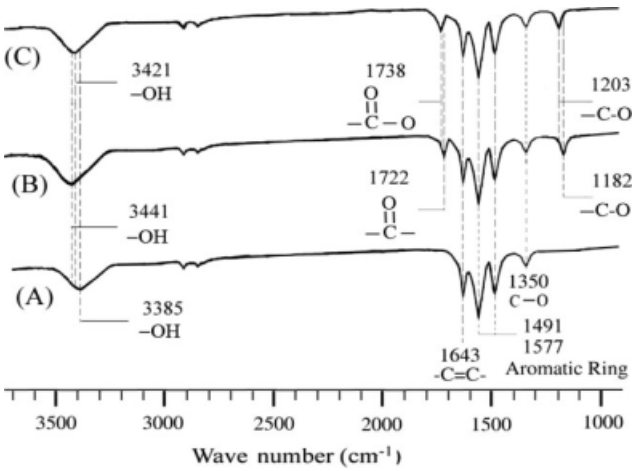

Figure 1 FTIR spectra for (A) MWNT, (B) MWNT–COOH, and (C) MWNT–OH.

PC spectrophotometer (Hitachi, Tokyo, Japan). Glass transition (T_g) and melting temperatures (T_m) were determined using a 2010 DSC system (TA Instruments, New Castle, DE). Sample sizes ranged from 4 to 6 mg and melting curves were obtained between –30°C and 250°C at a heating rate of 10°C/min. The values of T_g and T_m were determined from the temperature and area of melting peaks in the differential scanning calorimetry (DSC) heating thermograms. A thermogravimetric analyzer (2010 TGA; TA Instruments) was used to assess whether organic–inorganic phase interactions influenced thermal degradation in hybrid samples. Samples were placed in alumina crucibles and subjected to a thermal ramp from 30°C to 500°C at a heating rate of 20°C/min. Initial decomposition temperatures (IDTs) were obtained at the shoulder of the mass loss (TG%) curve. To obtain transmission electron microscopy (TEM) micrographs, samples were mounted in epoxy resin and sliced on a microtome to create specimens of 60–100 nm thickness. Micrographs were acquired with a transmission electron microscope (JEM-100CX II; JEOL, Tokyo, Japan) at an acceleration voltage of 100 kV. In accordance with method ASTM D638, an Instron mechanical tester (Model Lloyd, LR5K type; Segensworth, Fareham, UK) was used to measure the tensile strength and strain at break using a 20 mm/min crosshead speed. Five measurements were performed for each sample, and the results were averaged to obtain a mean value.

RESULTS AND DISCUSSION

FTIR analysis

Figure 1 shows FTIR spectra of raw and functionalized MWNT from 1000 to 4000 cm^{-1}. Characteristic peaks of MWNTs can be observed at 1350 cm^{-1} (C—O), 1450–1600 cm^{-1} (aromatic ring), 1643 cm^{-1} (C=C), and 3385 cm^{-1} (—OH) in Figure 1(A). Two additional peaks at 1182 cm^{-1} and 1722 cm^{-1}, attributable to stretching vibrations of C=O and C—O groups of —COOH, respectively, are seen in the FTIR spectrum of MWNT–COOH in Figure 1(B). This result is in agreement with the findings of Huang et al.[33] and indicates that long ropes of MWNT were cleaved into short, open-ended pipes and that ends and sidewalls of the short pipes were covered with oxygen-containing functional groups, such as carboxyls (—COOH), carbonyls (—C=O), and hydroxyls (—OH), following chemical oxidation.[34]

Hydroxyl groups (—OH) were grafted onto the surface of MWNTs by a reaction of ethylene glycol and MWNT–COCl. These hydroxyls were then coupled to the —COOH group of PTT-*g*-AA by an esterification reaction to yield high-performance polymer nanocomposites, as shown in Scheme 1. Theoretically, the distinctive stretching vibration of —COCl should have been observed in the FTIR spectrum of MWNT–COCl. However, the characteristic transitions of —COCl were difficult to detect since the measurements were performed in air and the high hydrolytic reactivity resulted in immediate conversion of —COCl to carboxylate groups. Therefore, FTIR evidence of MWNT–COCl was not directly observed.

In the FTIR spectrum of MWNT–OH, shown in Figure 1, the C=O and —C—O stretching vibrations of ester groups shifted from 1722 cm^{-1} and 1182 cm^{-1} to 1738 cm^{-1} and 1203 cm^{-1}, respectively, as compared with the same transitions in Figure 1(B).[35,36] This observation confirmed that the —COCl group of MWNT–COCl reacted with ethylene glycol to form MWNT–OH. The hydroxyl stretching band appeared as a strong, broad band at 3385 cm^{-1} in crude MWNTs but shifted to 3441 cm^{-1} and 3426 cm^{-1} in samples of MWNT−COOH and MWNT−OH, respectively. The band at 3426 cm^{-1} was assigned to octahedral vacancies and designated to MWNT−OH. This region at 3200–3500 cm^{-1} is, therefore, representative of non-hydrogen-bonded hydroxyl groups (labeled as isolated or free hydroxyl groups).

The FTIR spectra of PTT, PTT-*g*-AA, PTT/MWNT, and PTT-*g*-AA/MWNT–OH are shown in Figure 2. The characteristic peaks of PTT at 1700–1750 and 500–1500 cm^{-1} were observed in neat PTT and PTT-*g*-AA.[37,38] An additional peak at 1711 cm^{-1}, assigned to —C=O, and a broad O—H stretching transition at 3218 cm^{-1} were observed in the modified PTT. The shoulder near 1711 cm^{-1} was attributable to free acid in the modified polymer. This pattern of distinctive peaks indicated successful grafting of AA to PTT. Similar results have been reported previously.[39,40] Figure 2 shows that the characteristic

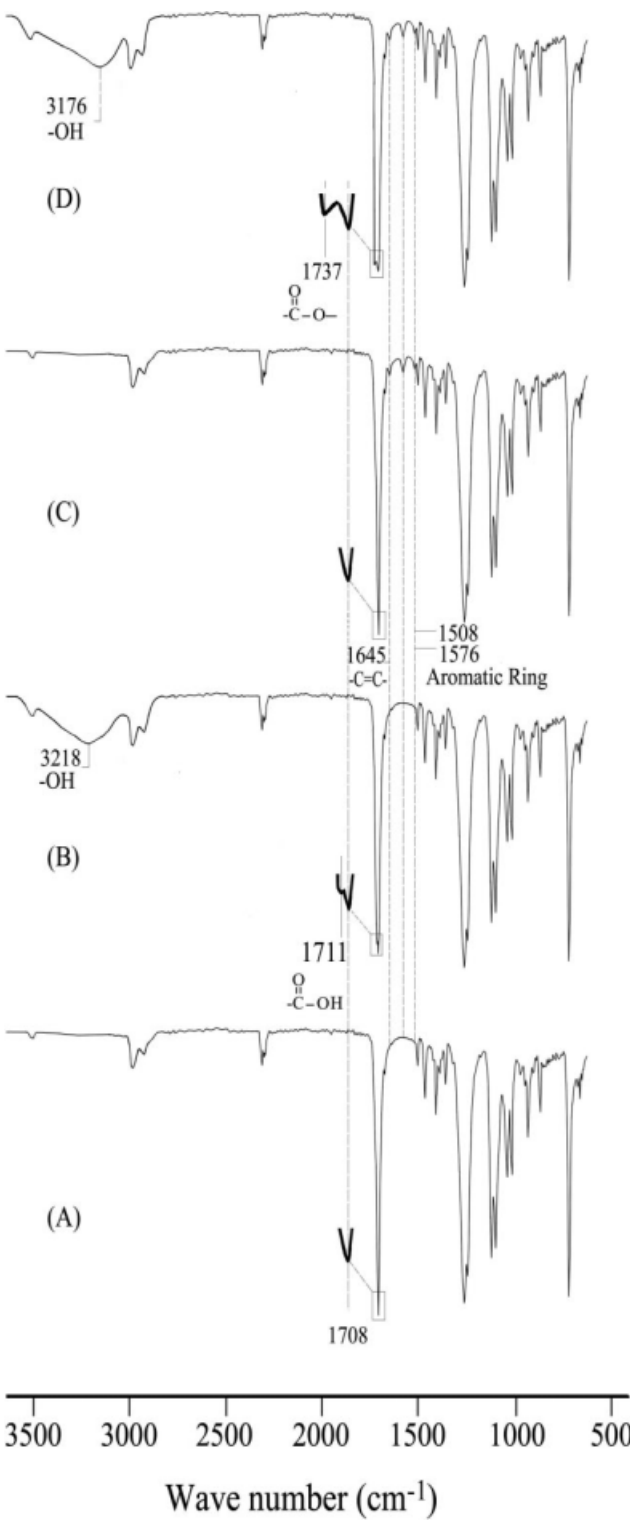

Figure 2 FTIR spectra for (A) PTT, (B) PTT-*g*-AA, (C) PTT/MWNT (1 wt %), and (D) PTT-*g*-AA/MWNT–OH (1 wt %).

FTIR peaks of PTT and MWNT were practically unchanged in the PTT/MWNT hybrid, indicating only physically dispersion of the nanotubes in the polymer matrix with no chemical interaction. In contrast, the FTIR spectrum of the MWNT–CO—O—$(CH_2)_2$—O—OC—PTT hybrid in Figure 2(D) shows that the peak at 1711 cm^{-1} in Figure 2(B) shifted to 1737 cm^{-1} as a result of condensation and ester formation between the carboxylic acid groups of PTT-*g*-AA and the hydroxyl groups of MWNT–OH. The hydroxyl stretching band of the PTT-*g*-AA copolymer appeared as a strong, broad band at 3218 cm^{-1} in Figure 2(B) but was shifted to 3176 cm^{-1} in the PTT-*g*-AA/MWNTs–OH hybrid due to the presence of H_2O from the esterification of PTT-*g*-AA and MWNT–OH.

NMR analysis

Further evidence for ester formation is provided by the ^{13}C NMR spectra shown in Figure 3. The ^{13}C NMR spectrum of neat PTT [Fig. 3(A)] was similar to that measured by Kameda et al.[41] and exhibited five peaks: (a) $\delta = 27.8$ ppm, (b) $\delta = 62.5$ ppm, (c) $\delta = 129.7$ ppm, (d) $\delta = 133.8$ ppm, and (e) $\delta = 165.6$ ppm. Relative to neat PTT, the ^{13}C NMR spectrum of PTT-*g*-AA [Fig. 3(B)] contained three additional peaks: (g) $\delta = 35.6$ ppm, (f) $\delta = 42.2$ ppm, (h) $\delta = 175.1$ ppm. These peaks confirmed the grafting of AA onto PTT as illustrated in Figure 3(B). The ^{13}C NMR spectrum of the PTT/MWNT, shown in Figure 3(C), also exhibited peaks not observed in neat PTT, corresponding to aromatic carbon atoms in the MWNT ($\delta = 120$–125 ppm). Peaks (i) and (j) [Fig. 3(D)], originating from the reaction between —COOH in PTT-*g*-AA and —OH in MWNT–OH, were found at $\delta = 177.1$ ppm and $\delta = 178.7$. These results, combined with the presence of FTIR peaks at

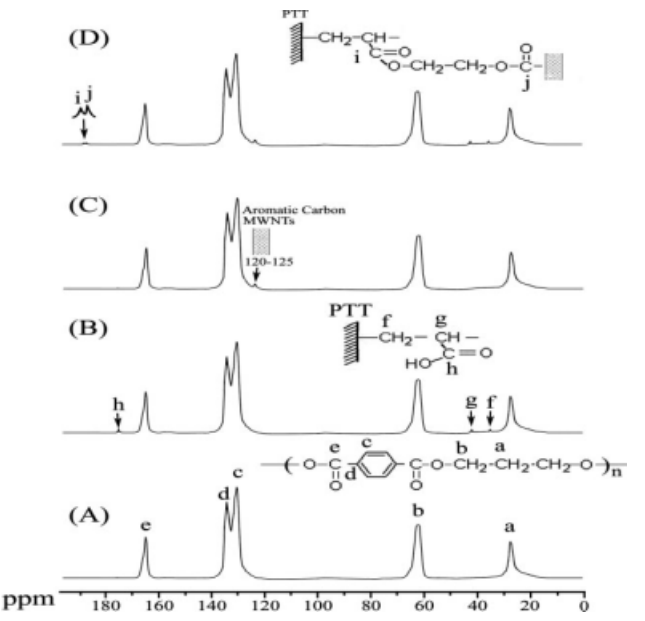

Figure 3 ^{13}C solid-state NMR spectra for (A) PTT, (B) PTT-*g*-AA, (C) PTT/MWNT (1 wt %), and (D) PTT-*g*-AA/MWNT–OH (1 wt %).

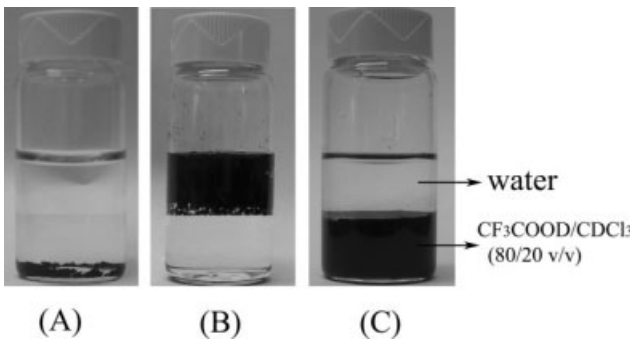

Figure 4 Dispersion of (A) pure MWNT, (B) MWNT-OH, (C) PTT-*g*-AA/MWNT–OH in a water (100%)/CF_3COOD/$CDCl_3$ (80/20 v/v) solution.

1737 cm^{-1} provide further evidence of ester group formation via condensation of PTT-*g*-AA with MWNTs–OH and support the hypothesis that the original MWNT−OH was fully hydroxylated and converted to ─COOR. The formation of these ester linkages had a profound effect on the thermal and mechanical properties of the hybrid composites and are discussed below.

Solubility and UV-vis analysis

To further demonstrate covalent linkage between PTT-*g*-AA and MWNT-OH, dispersibility of various samples in a mixture of H_2O and $CF_3COOD/CDCl_3$ was also tested. Note that the mixture would separate into upper phase (H_2O) and lower phase ($CF_3COOD/CDCl_3$). In Figure 4(A), it was found the pristine MWNT could not disperse in both solvents. However, the dispersibility of MWNT–OH in water was remarkably better due to the hydrophilic property of MWNT–OH [Fig. 4(B)]. Whilst for PTT-*g*-AA/MWNT–OH, because its hydrophobic polymer chains were soluble in $CF_3COOD/CDCl_3$, the covalent-linked MWNT–OH could instead well disperse in the organic phase [Fig. 4(C)].

Alternatively, *in situ* UV-vis absorbance spectra and digital photos of MWNT–OH, PTT/MWNT (1 wt %). PTT-*g*-AA/MWNT–OH (1 wt %). and PTT-*g*-AA/MWNT–OH (2 wt %) placed in the $CF_3COOD/CDCl_3$ solution were also shown in Figure 5. For line A in Figure 5, it formed a clear solution due to almost no absorption from 300 to 800 nm, indicating MWNT–OH was practically insoluble in the $CF_3COOD/CDCl_3$. For other composites (PTT/MWNT or PTT-*g*-AA/MWNT–OH), they become increasingly soluble in the $CF_3COOD/CDCl_3$ because of the increasing binding ability between PTT and MWNT or PTT-*g*-AA and MWNT–OH. *In situ* UV-vis analysis showed apparent absorbance intensity at about 380 nm for the composites (Lines B, C, and D in Fig. 5). Moreover, PTT/MWNT (1 wt %) samples contained more precipitate, and exhibited a lower absorbance, than samples of PTT-*g*-AA/MWNT–OH (1 wt %). The presence of covalent links between constituents likely enhanced the dispersibility of PTT-*g*-AA/MWNT–OH (1 wt %) over that of PTT/MWNT (1 wt %). Additionally, the 2 wt % PTT-*g*-AA/MWNT–OH sample resulted in more aggregation following hydrolysis in the $CF_3COOD/CDCl_3$ solution than the corresponding 1 wt % sample. This was likely due to greater dispersion in the 2 wt % sample.

Thermal properties of blends

The thermal properties of hybrid blends with varying MWNT–OH content were determined by DSC and thermal gravimetric analyses (TGA). The results are summarized in Figures 6 and 7. The T_gs of PTT-*g*-AA/MWNT–OH were higher than those of the PTT-*g*-AA copolymer (Fig. 6). The T_g of the hybrid composites can be associated with the cooperative motion of long-chain segments. These results suggest that the enhancement in T_g of PTT-*g*-AA/MWNT–OH hybrid blends was a result of ester formation between the hydroxyl groups of MWNT–OH and the carboxylic acid groups of PTT-*g*-AA, which hindered the relative motion of the polymer chains.

Variation of T_g for MWNT–OH loading above 1 wt % was somewhat less than that below 1 wt %. This may have been due to low grafting percentages in the PTT-*g*-AA copolymer (about 5.52 wt %) because T_g is dependent on the number of carboxylate groups in the copolymer matrix that are available to bind with hydroxyl groups on MWNT–OH.[42] At greater than 1 wt % MWNT–OH, the carboxylate

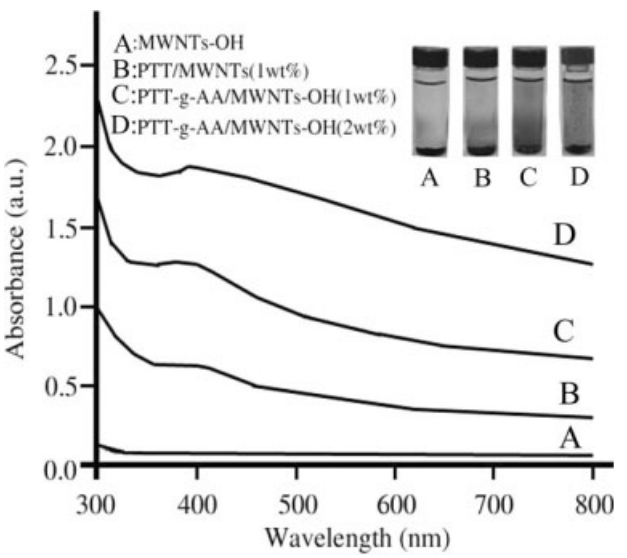

Figure 5 Absorption spectra for (A) MWNT–OH, (B) PTT/MWNT (1 wt %), (C) PTT-*g*-AA/MWNT–OH (1 wt %), and (D) PTT-*g*-AA/MWNT–OH (2 wt %) in a $CF_3COOD/CDCl_3$ (80/20 v/v) solution for 50 min.

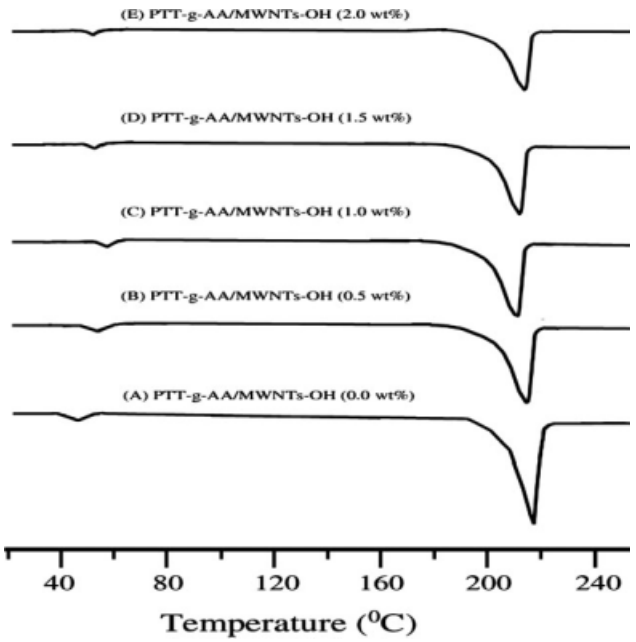

Figure 6 DSC heating thermograms of heating curves for PTT-*g*-AA and its blends with different degrees of MWNT–OH loading.

groups of PTT-*g*-AA were effectively saturated and the excess nanotubes physically dispersed in the polymer matrix without a chemical interaction. Excess MWNT–OH might have induced separation of the organic and inorganic phases by lowering compatibility, resulting in a slightly enhanced T_g.

Figure 6 also shows a marked decrease in T_m with increasing MWNT–OH content up to 1 wt % above which the T_m increase slightly again. The decrease in the T_m of PTT-*g*-AA/MWNT–OH was likely caused by inhibited polymer motion, which would prohibit the chain arrangement and reorganization required for solidification. Whilst the increase of T_m at content above 1 wt % was caused by the aggregation of excess MWNT–OH. T_g and T_m of the PTT/MWNT and PTT-*g*-AA/MWNT–OH hybrid materials were also summarized in Table I. As expected, both PTT/MWNT and PTT-*g*-AA/MWNT–OH exhibited higher T_gs than pure PTT. The enhancement in T_g was greater in PTT-*g*-AA/MWNT–OH than in PTT/MWNT. This was likely due to ester bond formation,

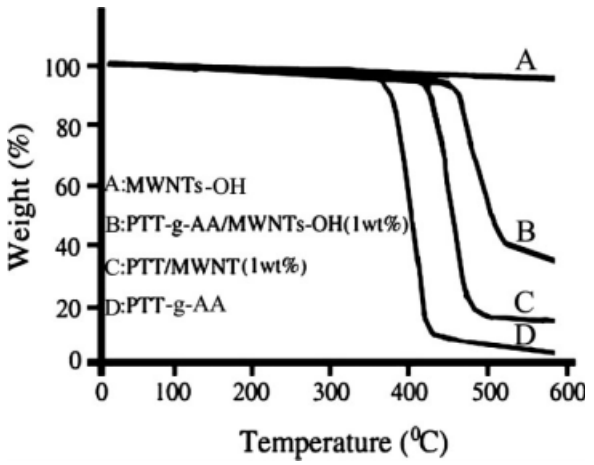

Figure 7 TGA analysis (in N_2) of (A) MWNT–OH, (B) PTT-*g*-AA/MWNT–OH (1 wt %), (C) PTT/MWNT (1 wt %), and (D) PTT-*g*-AA.

as discussed above. Ester linkages are stronger than the hydrogen bonds formed in PTT/MWNT and therefore more effective in hindering the motion of polymer chains. Moreover, T_m values for all PTT-*g*-AA/MWNT–OH hybrids were lower than their PTT/MWNT equivalents. This lower melting temperature of PTT-*g*-AA/MWNT–OH makes it a more easily processed blend. Conclusively, appearance of lowest T_m or highest T_g at 1 wt % demonstrates that an excess of MWNT or MWNT–OH content occurred at >1 wt%, which dispersed physically in the polymer matrix. Such excess MWNT or MWNT–OH might cause aggregation between the organic and inorganic phases, and lessen the compatibility between PTT/MWNT and PTT-*g*-AA/MWNT–OH.

Furthermore, prompted by the fact that CNTs can be defunctionalized by thermal decomposition, TGAs were performed to determine the effect of MWNT–OH loading on the weight loss of hybrid blends. The results are shown in Figure 7 and Table I. The IDTs of PTT-*g*-AA and hybrid blends with 1.0 wt % MWNT–OH content were 362°C and 451°C, respectively. MWNT–OH itself was not degraded at temperatures up to 500°C. The increase in IDT was likely caused by inhibition of molecular motion, as described above. Another potential cause is condensation reactions between MWNT–OH and PTT-*g*-

TABLE I
Thermal Properties of PTT/MWNT and PTT-*g*-AA/MWNT-OH

MWNTs or MWNT-OH (wt %)	PTT/MWNT			PTT-*g*-AA/MWNT-OH		
	IDT (°C)	T_g (°C)	T_m (°C)	IDT (°C)	T_g (°C)	T_m (°C)
0.0	379	49.2	219.1	362	45.1	218.2
0.5	392	52.5	217.9	420	55.3	215.9
1.0	410	53.9	216.5	451	58.9	213.8
1.5	415	51.8	217.1	459	54.8	214.8
2.0	421	50.5	217.8	466	52.9	215.6

AA. Kong et al.[43] studied the properties of polystyrene/MWNT nanocomposites and reported similar phenomena. According to the TGA traces in Figure 7, the IDT of PTT-*g*-AA increased by 89°C with the addition of 1 wt % MWNT–OH. The IDT was enhanced only another 15°C as the MWNT–OH content was increased from 1 to 2 wt %. This result further supports the above conclusion that optimal loading of MWNT–OH in PTT-*g*-AA occurs at 1 wt %. As previously noted, excess MWNT–OH decreased the constituent compatibility in the hybrid blends.

In addition, the residual mass of the PTT-*g*-AA/MWNT–OH nanocomposites increased with increasing MWNT–OH content. This may have been attributable to a physical barrier effect in which the MWNT–OH prevented the transport of decomposition products. Similar results have been reported whereby the thermal stability of polypropylene/MWNT nanocomposites was improved by a physical barrier effect and enhanced by ablative reassembling of the MWNT layer.[44] The TGA results demonstrated that the incorporation of a small quantity of MWNT–OH can markedly improve the thermal stability of PTT-*g*-AA/MWNT–OH nanocomposites. As to the results in Table I, the IDT values were higher in both the PTT/MWNT and PTT-*g*-AA/MWNT–OH hybrids. In addition, despite the lower IDT of PTT-*g*-AA relative to PTT, the PTT-*g*-AA/MWNT–OH hybrid materials exhibited higher IDT values than those of the equivalent PTT/MWNT blends. This outcome was a result of the difference in interfacial forces in the two hybrid materials: the weaker hydrogen bonds of PTT/MWNT relative to the stronger coordination sites associated with the carboxylic acid groups of PTT-*g*-AA and the –OH groups of MWNT–OH. Table I further showed that the change in IDT for both hybrid materials was not significant at a MWNT or MWNT–OH content above 1 wt %, which was also attributable to agglomeration at higher filler content (Fig. 8).

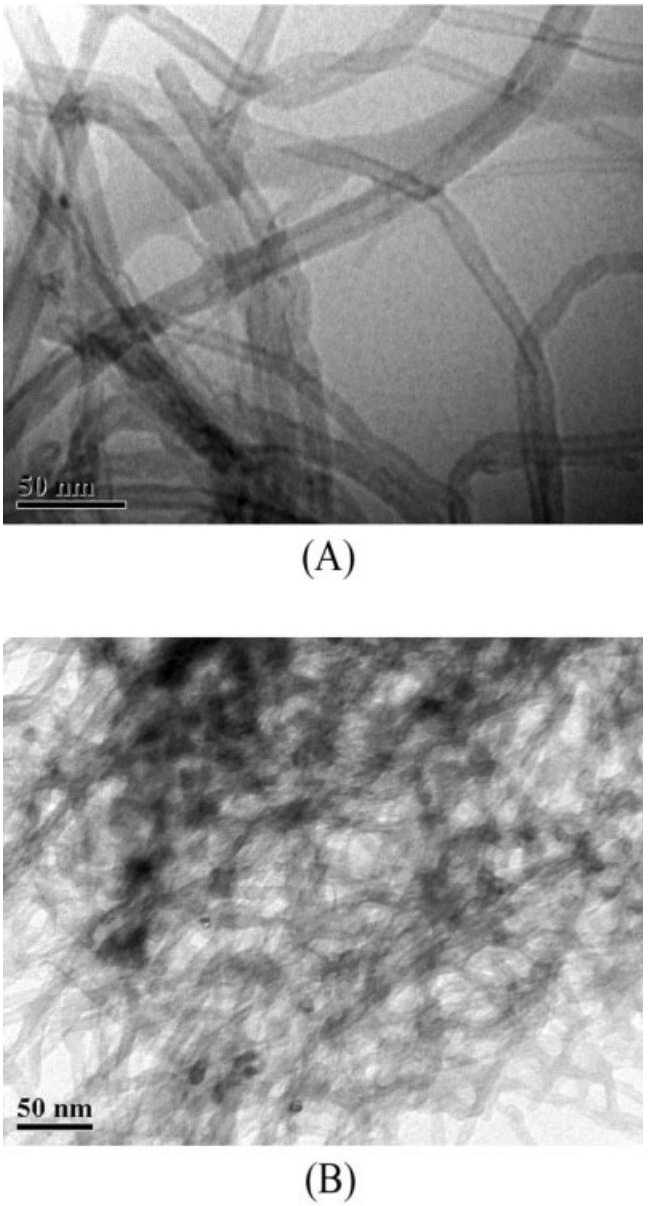

Figure 8 TEM micrographs for (A) PTT-*g*-AA/MWNT–OH (1 wt %) and (B) PTT-*g*-AA/MWNT–OH (2 wt %).

Hybrid morphology

The morphology of the MWNT–OH and polymer blends can be directly related to their mechanical properties. In general, good dispersion of MWNT–OH throughout the polymer matrix, effective functionalization of MWNT–OH, and strong interfacial adhesion between the two phases are required to obtain a composite material with satisfactory mechanical properties. Tensile fractured surfaces of PTT-*g*-AA/MWNT–OH blends were imaged with TEM. The resulting micrographs are shown in Figure 8. Individual embedded MWNT–OH tubes were difficult to locate in the polymer matrix when there were insufficient dispersion and poor interfacial adhesion between MWNT–OH and the polymer matrix. This resulted in the formation of MWNT–OH aggregates. As shown in Figure 8, MWNT–OH was evenly dispersed in the polymer matrix at a loading of 1 wt % but formed aggregates at 2 wt %.

Mechanical properties of hybrids

The variation in tensile strength at break (TS), elongation at break (EB) and initial modulus (IM), as a function of MWNT or MWNT–OH content in PTT/MWNT and PTT-*g*-AA/MWNT–OH, is shown in Table II. Maximum (TS and IM) or Minimum (EB) values for both PTT/MWNT and PTT-*g*-AA/MWNT–OH were realized at about 1 wt % MWNT and MWNT–OH. In PTT/MWNT, the effect of MWNT

TABLE II
Mechanical Properties of PTT/MWNT and PTT-*g*-AA/MWNT-OH

MWNT or MWNT-OH (wt %)	PTT/MWNT			PTT-*g*-AA/MWNT-OH		
	TS (MPa)	EB (%)	IM (GPa)	TS (MPa)	EB (%)	IM (GPa)
0.0	50.6 ± 1.3	12.5 ± 0.3	2.26 ± 0.03	45.8 ± 1.5	11.9 ± 0.4	2.08 ± 0.06
0.5	56.8 ± 1.5	11.6 ± 0.4	2.46 ± 0.04	70.6 ± 1.8	8.3 ± 0.5	2.86 ± 0.05
1.0	61.6 ± 1.6	10.5 ± 0.5	2.65 ± 0.05	82.6 ± 1.9	4.9 ± 0.6	3.32 ± 0.06
1.5	57.1 ± 1.8	10.8 ± 0.6	2.53 ± 0.07	72.3 ± 2.1	6.7 ± 0.7	2.98 ± 0.08
2.0	53.8 ± 1.9	11.2 ± 0.7	2.43 ± 0.08	65.6 ± 2.3	7.8 ± 0.8	2.78 ± 0.09

content on the tensile strength was slight due to the lack of bonding between the PTT matrix and the MWNT. PTT-*g*-AA/MWNT–OH, with the same MWNT or MWNT–OH loading, exhibited a much higher tensile strength than PTT/MWNT, despite the lower tensile strength of the PTT-*g*-AA copolymer relative to pure PTT. This enhancement may have been attributable to the presence of MWNT–OH and the formation of ester linkages, as discussed above. Although the tensile strength of PTT-*g*-AA/MWNT–OH increased to about 82.6 MPa at 1 wt % MWNT–OH, it decreased considerably at higher MWNT–OH loading, likely due to separation between the organic and inorganic phases.

The positive effect on tensile strength may have been due to several factors, including the stiffness of the MWNT−OH layers contributing to the presence of immobilized or partially immobilized polymer phases,[45] the high aspect ratio and surface area of the CNTs, and the nanoscale dispersion of MWNT−OH layers in the polymer matrix. In addition, the orientation of the MWNT−OH layer, as well as the molecular orientation of individual MWNT–OH, may have contributed to the observed reinforcement effect. The slight decrease in tensile strength at MWNT−OH loading above 1 wt % may have been attributable to aggregation of MWNT−OH. These results support the theoretical and molecular simulation predictions that stress transfer, and hence the strength of the composites, can be effectively increased by the formation of chemical bonds between the nanotubes and the polymer matrix.[46,47]

CONCLUSIONS

MWNTs were functionalized using a simple method and used to prepare high-performance PTT nanocomposites. The MWNT−OH was covalently incorporated into a PTT-*g*-AA copolymer through the formation of strong ester bonds produced from condensation of the carboxylic acid groups of PTT-*g*-AA and the hydroxyl groups of MWNT–OH. FTIR spectra and ^{13}C solid-state NMR showed that the AA moiety had been grafted onto the PTT copolymer and that ester bonds had formed in the PTT-*g*-AA/MWNT–OH hybrid material. PTT-*g*-AA/MWNT–OH exhibited greatly increased suspendibility in the $CF_3COOD/CDCl_3$ due to the high solubility of polymer chains and the covalent linkage between the constituents. TEM micrographs of the nanocomposites showed the formation of CNT aggregates at high MWNT–OH loading. DSC analysis found that the gap between T_g and T_m of the PTT-*g*-AA/MWNT–OH hybrid was smaller than that of the PTT/MWNT. This implies that the compatibility between PTT and MWNT had been enhanced. TGAs showed that the incorporation of 1 wt % MWNT–OH into PTT-*g*-AA increased the initial decomposition temperature by 89°C. Maximum tensile strength of all hybrid materials occurred at about 1 wt % of MWNT–OH. Excess MWNT–OH reduced the compatibility of the hybrid due to the aggregation of CNTs. Thus, MWNT−OH can play a reinforcement role in the PTT-*g*-AA polymer matrices.

References

1. Liu, W.; Mohanty, A. K.; Drzal, L. T.; Misra, M.; Kurian, J. V.; Miller, R. W.; Strickland, N. Ind Eng Chem Res 2005, 44, 857.
2. Huang, J. M. J Appl Polym Sci 2003, 88, 2247.
3. Grebowicz, J. S.; Brown, H.; Chuah, H.; Olvera, J. M.; Wasiak, A.; Sajkiewicz, P.; Ziabjacki, A. Polymer 2001, 42, 7153.
4. Guerrica-Echevarria, G.; Eguiazabal, J. I.; Nazabal, J. Eur Polym J 2007, 43, 1027.
5. Wu, T.; Li, Y.; Wu, Q.; Song, L.; Wu, G. Eur Polym J 2005, 41, 2216.
6. Kelsey, D. R.; Kiibler, K. S.; Tutunjian, P. N. Polymer 2005, 46, 8937.
7. Yamen, M.; Ozkaya, S.; Vasanthan, N. J Polym Sci Part B: Polym Phys 2008, 46, 1497.
8. Ho, R. M.; Ke, K. Z.; Chem, M. Macromolecules 2000, 33, 7529.
9. Gonzalez, I.; Eguiazabal, J. I.; Nazabal, J. J Appl Polym Sci 2008, 108, 3828.
10. Ou, C. F. Eur Polym J 2002, 38, 2405.
11. Farmahini-Farahani, M.; Jafari, S. H.; Khoonakdar, H. A.; Yavari, A.; Bakhshi, R.; Tarameshlou, M. Macromol Mater Eng 2007, 292, 1103.
12. Chang, J.-H.; Kim, S. J.; Im, S. Polymer 2004, 45, 5171.
13. Kim, K. J.; Ramasundaram, S.; Lee, J. S. Polym Comp 2008, 29, 894.
14. Zha, W.; Choi, S.; Lee, K. M.; Han, C. D. Macromolecules 2005, 38, 8418.
15. Vaia, R. A.; Ishii, H.; Giannelis, E. P. Chem Mater 1993, 5, 1694.

16. Jang, B. N.; Wang, D.; Wilkie, C. A. Macromolecules 2005, 38, 6533.
17. Iijima, S. Nature 1991, 354, 56.
18. Yao, Z.; Braidy, N.; Botton, G. A.; Adronov, A. J Am Chem Soc 2003, 125, 16015.
19. Xie, L.; Xu, F.; Qiu, F.; Lu, H.; Yang, Y. Macromolecules 2007, 40, 3296.
20. Mansfield, M. L.; Douglas, J. Macromolecules 2008, 41, 5412.
21. Koval'chuk, A. A.; Shevchenko, V. G.; Shchegolikhin, A. N.; Nedorezova, P. M.; Klyamkina, A. N.; Aladyshev, A. M. Macromolecules 2008, 41, 7536.
22. Liu, I. C.; Huang, H. M.; Chang, C. Y.; Tsai, H. C.; Hsu, C. H.; Tsiang, R. C. C. Macromolecules 2004, 37, 283.
23. Hu, H.; Ni, Y.; Montana, V.; Haddon, R. C.; Parpura, V. Nano Lett 2004, 4, 507.
24. Lin, J.; Rinzler, A. G.; Dai, H.; Hafner, J. H.; Bradley, R. K.; Boul, P. J.; Lu, A.; Iverson, T.; Shelimov, K.; Huffman, C. B.; Rodriguez-Macias, F.; Shon, Y. S.; Lee, T. R.; Colbert, D. T.; Smalley, R. E. Science 1998, 280, 1253.
25. Gao, J.; Zhao, B.; Itkis, M. E.; Bekyarova, E.; Hu, H.; Kranak, V.; Yu, A.; Haddon, R. C. J Am Chem Soc 2006, 128, 7492.
26. Chen, J.; Hamon, M. A.; Hu, H.; Chen, Y.; Rao, A. M.; Eklund, P. C.; Haddon, R. C. Science 1998, 282, 95.
27. Zeng, H. L.; Gao, C.; Yan, D. Y. Adv Funct Mater 2006, 16, 812.
28. Forrest, G. A.; Alexander, A. J. J Phys Chem C 2007, 111, 10792.
29. Zhu, J.; Peng, H.; Fernando, R. M.; Margrave, J. L.; Khabashesku, V. N.; Imam, A. M.; Lozano, K.; Barrera, E. V. Adv Funct Mater 2004, 14, 643.
30. Sano, M.; Kamino, A.; Okamura, J.; Shinkai, S. Langmuir 2001, 17, 5125.
31. Wu, C. S. Macromol Biosci 2005, 5, 352.
32. Wang, Z.; Chen, Y. Macromolecules 2007, 40, 3402.
33. Huang, H. M.; Lin, I. C.; Chang, C. Y.; Tsai, H. C.; Hsu, C. H.; Tsiang, R. C. J Polym Sci A 2004, 42, 5802.
34. Tobias, G.; Shao, L.; Salzmann, C. G.; Huh, Y.; Green, M. L. H. J Phys Chem B 2006, 110, 22318.
35. Besteman, K.; Lee, J. O.; Wiertz, F. G. M.; Heering, H. A.; Dekker, C. Nano Lett 2003, 3, 727.
36. Han, J. T.; Kim, S. Y.; Woo, J. S.; Jeong, H. J.; Oh, W.; Lee, G.-W. J Phys Chem C 2008, 112, 15961.
37. Chuah, H. H. Macromolecules 2001, 34, 6985.
38. Seo, Y. W.; Pang, K.; Kim, Y. H. Macromol Mater Eng 2006, 291, 1327.
39. Kim, J.; Tirrell, D. A. Macromolecules 1999, 32, 945.
40. Wu, C. S.; Liao, H.-T. Polymer 2005, 46, 10017.
41. Kameda, T.; Miyazawa, M.; Murase, S. Macromol Reson Chem 2005, 43, 21.
42. Xu, Y.; Gao, C.; Kong, H.; Yan, D.; Jin, Y. Z.; Watts, P. C. P. Macromolecules 2004, 37, 8846.
43. Kong, H.; Gao, C.; Yan, D. Macromolecules 2004, 37, 4022.
44. Bom, D.; Andrews, R.; Sreekumar, T. V.; Kumar, S.; Moore, V. C.; Hauge, R. H.; Smalley, R. E. Nano Lett 2002, 2, 615.
45. Zhang, X.; Liu, T.; Sreekumar, T. V.; Kumar, S.; Moore, V. C.; Hauge, R. H.; Smalley, R. E. Nano Lett 2003, 3, 1285.
46. Liu, L.; Barber, A. H.; Nuriel, S.; Wagner, H. D. Adv Funct Mater 2005, 15, 975.
47. Geng, H.; Rosen, R.; Zheng, B.; Shimoda, H.; Fleming, L.; Liu, J.; Zhou, O. Adv Mater 2002, 14, 1387.